Journal of Geoscience and Environment Protection, 2026, 14(5), 333-350
https://www.scirp.org/journal/gep
ISSN Online: 2327-4344
ISSN Print: 2327-4336

Research on the Mechanism of Intense Variation in the Strength of Super Typhoon "Yagi" and Analysis of Its Causes

Weiyi Zeng, Guangze Gao*, Hongze Leng

College of Meteorology and Oceanography, National University of Defense Technology, Changsha, China
Email: *76210515@qq.com

How to cite this paper: Zeng, W. Y., Gao, G. Z., & Leng, H. Z. (2026). Research on the Mechanism of Intense Variation in the Strength of Super Typhoon "Yagi" and Analysis of Its Causes. *Journal of Geoscience and Environment Protection, 14,* 333-350.
https://doi.org/10.4236/gep.2026.145018

Received: April 29, 2026
Accepted: May 26, 2026
Published: May 29, 2026

Abstract

Typhoon "Yagi", the 11th super typhoon of 2024, underwent extreme explosive intensification in the northern part of the South China Sea, setting a record for the duration of a super typhoon in the South China Sea area and posing significant disaster risk. Based on ERA5 reanalysis data, Fengyun-4B (FY-4B) satellite, Doppler radar, and typhoon optimal path data, this study employed the coupled diagnostic of dynamics and thermodynamics, three-dimensional wind field decomposition in cylindrical coordinates, and vertical weighting of guiding airflow to analyze the mechanism of intensity abnormal evolution, the response of the core structure, and the path control factors. The results show that "Yagi" has an optimal dynamic configuration of strong positive vorticity in the lower layers and weak negative vorticity in the upper layers, strong convergence in the lower layers and strong divergence in the upper layers; the warming structure from 300 to 500 hPa is deep, combined with the spiral humidity distribution to form a stable thermal support; the eye wall wind field and intensity outbreak height are coupled, weak environmental vertical wind shear ensures the axisymmetric structure; the easterly guiding airflow dominates the path, and the abnormal warm sea surface temperature in the South China Sea continuously supplies energy. This study can provide theoretical and technical support for the forecast and warning of super typhoons in the South China Sea during the autumn season.

Keywords

Super Typhoon "Yagi", Explosive Intensification, Dynamic-Thermal Coupling, Steering Airflow

1. Introduction

Super Typhoon "Yagi" (No. 11 of 2024) was the strongest autumn typhoon to

make landfall in China since 1981, and it also holds the record for the longest duration at super typhoon intensity in the South China Sea since records began (Yang et al., 2026). The typhoon formed over the waters east of Philippines on September 1, then moved northwestward, crossing Luzon Island and entering the South China Sea. In the northern South China Sea, it underwent three significant rapid intensification events, one of which met the criteria for extreme rapid intensification; both the 12-hour and 24-hour intensity increases were the highest recorded for a South China Sea typhoon since 1981. "Yagi" maintained super typhoon intensity for 64 hours, far exceeding the second-longest duration recorded by Typhoon "Sura" (48 hours). Its peak intensity reached 68 m/s (Category 17 or higher). It made landfall successively in Wenchang, Hainan; Xuwen, Guangdong; and Quang Ninh, Vietnam, causing extremely severe wind and rain disasters in South China and the Indochinese Peninsula.

Accurate forecasting of typhoon intensity and track is crucial for disaster prevention and mitigation; however, rapid intensification (RI) and track anomalies remain major challenges in current international typhoon forecasting (Chen & Ding, 1979). In recent years, although numerical forecast models have made significant progress in typhoon track forecasting, there remains considerable uncertainty regarding the mechanisms of intensity changes and the dominant factors influencing the tracks of rapidly intensifying typhoons in the South China Sea, particularly strong autumn typhoons (Yan et al., 1995). Previous studies have shown that ample water vapor supply, weak environmental vertical wind shear, high sea surface temperatures, and favorable upper-level outflow are key external conditions for rapid typhoon intensification (Liang & Cheng, 2017); meanwhile, the typhoon's internal positive vorticity column, warm-core structure, and kinetic energy budget processes determine its intensification potential (Yu et al., 2007). However, for a rare typhoon like "Yagi", which simultaneously exhibited extremely rapid intensification, sustained super-intense strength for an extended period, and a stable, westward-biased track, existing studies have largely focused on single aspects (such as atmospheric circulation or oceanic heat flux), lacking a systematic, integrated analysis of its dynamic, thermal, and structural evolution as well as steering flow mechanisms (Liang & Wu, 1986). Furthermore, the fractal characteristics of satellite remote sensing imagery provide a new quantitative perspective on the complexity of typhoon structure (Chen et al., 2026), while the systematic bias in numerical model forecasts of "Yagi"'s early track also urgently requires attribution (Wu et al., 2026).

Based on the above issues, this study comprehensively utilizes data from ground-based observations, sounding data, the Fengyun-4B (FY4B) satellite, Doppler weather radar, and ERA5 reanalysis data. By combining methods such as columnar coordinate interpolation, kinetic energy budget diagnostics, fractal dimension calculations, and steering flow analysis, this study systematically investigates the characteristics of the anomalous intensity variations of Super Typhoon "Yagi" during its activity in the South China Sea and their underlying causes (Velden & Leslie, 1991). The study focuses on addressing the following scientific questions: 1) The three-dimensional structural evolution of the dynamic field (vorticity, divergence) and

thermal field (warm core, humidity) during the three rapid intensification episodes of "Yagi"; 2) The quantitative characteristics of tangential winds, radial flow, and vertical motion in the typhoon's eyewall region, and their response to intensity changes; 3) Changes in the vertical weighting of the steering flow and the control mechanisms governing the stable westerly track; The research findings aim to provide a theoretical basis and technical reference for intensity forecasting and track warnings of super typhoons in the South China Sea during the autumn season.

2. Innovative Approaches and Methods in Analysis

Previous studies on typhoons in the South China Sea have largely relied on traditional methods such as single-field diagnostics, two-dimensional planar analysis, and single-level steering flow calculations. These approaches have not achieved three-dimensional quantitative diagnostics that couple dynamics and thermodynamics, nor have they eliminated the interference of the typhoon's core circulation on the environmental field, making it difficult to capture the subtle structural features of the extreme intensification of Typhoon "Yagi". Building upon conventional methods, this paper offers some innovative methods and perspectives.

2.1. Two-Factor Objective Localization and Ring-Band Subtraction Method

Overcoming the limitations of traditional single-factor positioning, this method employs a dual-verification approach—combining the minimum sea-level pressure with the maximum relative vorticity at 850 hPa—to locate the typhoon center, thereby avoiding manual positioning errors (Toyoda et al., 2025); Simultaneously, environmental field parameters are calculated using a circular zone with a latitudinal and longitudinal radius of 3˚ - 7˚ around the typhoon center, completely eliminating interference from the typhoon's own circulation (Oh et al., 2015). This approach aligns with the precise paradigm for analyzing the environmental field of tropical cyclones and resolves the issue of diagnostic distortion in the environmental field caused by traditional methods (Ford & Kench, 2016).

$$\begin{cases} P_s\left(x_0,y_0\right)=\min\left\{P_s\left(x,y\right)\right\},\left(x,y\right)\in D & (1)\\ \varepsilon_{850}\left(x_0,y_0\right)=\max\left\{\varepsilon_{850}\left(x,y\right)\right\},\left(x,y\right)\in D & (2)\\ P_s\left(x_0,y_0\right)\le 1000hPa & (3)\end{cases}$$

Equation (1) P_s is sea-level pressure (hPa); ε_{850} is the relative vorticity at 850 hPa (10^{-5}·s^{-1}); D is the typhoon search area; and $\left(x_0,y_0\right)$ are the coordinates of the typhoon's center.

2.2. Three-Dimensional Wind Field Decomposition in a Cylindrical Coordinate System and Quantitative Profiling of the Eye Wall

Interpolate the wind field from the Cartesian coordinate system to the cylindrical coordinate system (r, θ, p), accurately decomposing the tangential wind, radial wind, and vertical motion; the interpolation method used is bilinear interpolation,

with a radial resolution of 10 km and an azimuthal resolution of 10˚. The tangential wind (V_t) and radial wind (V_r) in the cylindrical coordinate system are calculated using the following formulas:

$$V_t = -u\sin\theta + v\cos\theta \tag{4}$$

$$V_r = v\sin\theta + u\cos\theta \tag{5}$$

In Equation (4), the radial wind is negative when it flows towards the center. The vertical velocity (ω, unit: hPa·s^{-1}) is directly taken from ERA5, and the ascending motion is negative.

For the first time, a daily quantitative statistics was conducted in the core area of the eye wall ranging from 70 to 100 kilometers. This enabled a clear identification of the coupling relationship between wind field sudden changes and intensity bursts, compensating for the previous lack of comprehensive wind field analysis and the neglect of the key core area.

2.3. Dynamics, Thermal Vertical Stratification Coupling Diagnosis

Break through the limitations of single dynamic field or thermal field analysis, conduct vertical layer-by-layer coupling analysis of vorticity, divergence, warm core, and humidity, reveal the "cooperative enhancement mechanism of mid-low level dynamic driving and mid-high level thermal support", and clearly depict the three-dimensional physical process of rapid typhoon intensification (Ford & Kench, 2014).

2.4. Analysis of the Combined Effect of the Entire-Layer Weighted Guiding Airflow and Multi-System Circulation

The guiding airflow of the entire layer is calculated by weighting the 500 hPa and 850 hPa data equally. The environmental vertical wind shear is defined as the difference in the horizontal wind vectors between 200 hPa and 850 hPa. The calculation formula is:

$$V_{shear} = \sqrt{\left(\overline{u_{200}} - \overline{u_{850}}\right)^2 + \left(\overline{v_{200}} - \overline{v_{850}}\right)^2} \tag{6}$$

In Equation (6), $\overline{u}$ and $\overline{v}$ represent the area-averaged meridional wind and zonal wind within a circular area of 3˚ to 7˚ latitude distance from the center of the typhoon. This definition can shield the influence of strong winds in the typhoon core on the estimation of shear. By combining the analysis of multiple systems of the subtropical high, continental high, and South Asian high circulation, it accurately explains the cause of the stable westward path of "Yagi", solving the problem that traditional single-layer guiding airflow analysis cannot explain the absolute control of the path.

2.5. Cross-Validation Method for Reliability Testing

By integrating satellite cloud top temperature data, radar radial velocity data, ground observations and reanalysis data, and using the cross-validation method to verify the analysis results of typhoon intensity, structure and path, the reliability of the conclusions is enhanced.

1) Cross-validation of typhoon path: Average path error

$$\mathrm{APE} = \frac{1}{\mathrm{N}}\sum_{\mathrm{i}=1}^{\mathrm{N}} \arccos\left[\sin\varphi_i \sin\varphi_i' + \cos\varphi_i \cos\varphi_i' \cos\left(\lambda_i - \lambda_i'\right)\right] \cdot \mathrm{R} \tag{7}$$

In the equation, APE represents the average path error (km); φ, λ are the longitude and latitude of the optimal path; φ', λ' are the paths from reanalysis/inversion; R = 6371 km is the radius of the Earth; N is the number of samples.

2) Cross-validation of typhoon intensity: Mean absolute error and root mean square error

$$\mathrm{MAE} = \frac{1}{\mathrm{N}}\sum_{\mathrm{i}=1}^{\mathrm{N}} \left|\mathrm{V}_{\max,\mathrm{i}} - \mathrm{V}'_{\max,\mathrm{i}}\right| \tag{8}$$

$$\mathrm{RMSE} = \sqrt{\frac{1}{\mathrm{N}}\sum_{\mathrm{i}=1}^{\mathrm{N}} \left(\mathrm{V}_{\max,\mathrm{i}} - \mathrm{V}'_{\max,\mathrm{i}}\right)^2} \tag{9}$$

In Equation (8), $\mathrm{V}_{\max}$ represents the maximum wind speed of the optimal path; $\mathrm{V}'_{\max}$ represents the wind speed derived from radar/satellite measurements.

3) Cross-validation of typhoon structure parameters: Coefficient of consistency

$$\mathrm{IOA} = 1 - \frac{\sum_{\mathrm{i}=1}^{\mathrm{N}} \left(\mathrm{X}_{\mathrm{i}} - \hat{\mathrm{X}}_{\mathrm{i}}\right)^2}{\sum_{\mathrm{i}=1}^{\mathrm{N}} \left(\left|\mathrm{X}_{\mathrm{i}} - \bar{\mathrm{X}}\right| + \left|\hat{\mathrm{X}}_{\mathrm{i}} - \bar{\mathrm{X}}\right|\right)^2} \tag{10}$$

In Equation (10), X represents the observed or actual structural parameters (vorticity, divergence, tangential wind); $\hat{\mathrm{X}}$ represents the simulated values from reanalysis data; IOA ∈ [0, 1], the closer it is to 1, the better the consistency.

The aforementioned innovative method has achieved a leap from "two-dimensional qualitative" to "three-dimensional quantitative", and from "single-field analysis" to "coupled diagnosis". This is the core guarantee for this paper to reveal the extreme enhancement mechanism and path causes of "Yagi".

3. Experimental Data

This study utilizes multiple sources of data, including reanalysis data, satellite remote sensing products, radar observations, and the best track set of typhoons. The details are as follows:

1) Reanalysis data: The data set used is the Fifth Generation Global Atmospheric Reanalysis Dataset (ERA5) from the European Centre for Medium-Range Weather Forecasts (ECMWF). The time range is from 00:00 on September 1, 2024 to 18:00 on September 9 (Beijing time), with a spatial resolution of 0.25˚ × 0.25˚ and a temporal resolution of 1 hour. The selected pressure levels include 1000, 850, 700, 600, 500, 400, 300, 200, and 100 hPa. The physical quantities extracted include: potential height, horizontal wind components (u, v), vertical velocity (ω), temperature, relative humidity, sea surface temperature (SST), divergence, relative vorticity, and precipitation. This data set is used for diagnosing the typhoon environment field, analyzing the dynamic and thermodynamic structure, calculating the guiding airflow, and estimating the energy budget.

2) Satellite remote sensing data: The data of the black body brightness temperature (TBB) of typhoon cloud tops is obtained from the 9210 format product of

Fengyun-2H satellite (FY-2H). The time resolution is 1 hour, and the spatial coverage is from 30˚N to 30˚S and 80˚E to 160˚E. The data is sourced from the National Meteorological Information Center (https://data.cma.cn/).

3) Radar observation data: 0.5˚ elevation angle radial velocity products from Doppler weather radars in Haikou, Hainan Province and Fangchenggang, Guangxi Province, used to verify the maximum wind speed near the center.

4) Typhoon positioning and intensity data: The latitude and longitude of the center, the minimum central pressure, and the maximum wind speed near the center of Typhoon "Yagi" are taken from the Central Meteorological Administration (CMA) Typhoon Optimal Path Set (updated every 3 hours). This data is used for the verification of model forecast deviations and the phased division of the typhoon path.

Geographic base maps for **Figures 3-8** are official standard maps provided by the Standard Map Service System of the Ministry of Natural Resources of the People's Republic of China (http://bzdt.ch.mnr.gov.cn/), without any alteration to national boundaries, islands, and maritime demarcation lines.

4. Analysis of Abnormal Strength

4.1. Optimal Configuration of the Dynamic Field and Secondary Circulation Driving

During the super typhoon stage (from 06:00 on September 5th to 22:00 on September 6th), "Yagi" exhibited a vertical configuration of strong positive vorticity in the middle and lower levels and weak negative vorticity in the upper levels: the relative vorticity center value at 850 hPa reached 12 to 15 × 10^{-5}·s^{-1}, significantly higher than the threshold of an ordinary typhoon; at 500 hPa, it maintained 8 to 10 × 10^{-5}·s^{-1} positive vorticity, and at 200 hPa, it changed to −1 to −2 × 10^{-5}·s^{-1} weak negative vorticity, forming a continuous cyclonic rotational suction effect.

The divergence field presented a coupled characteristic of strong convergence in the lower levels and strong divergence in the upper levels: the convergence center

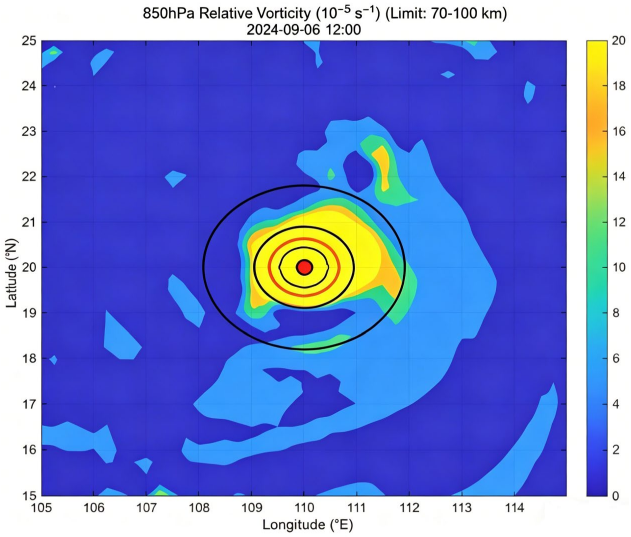

Figure 1. Relative vorticity map at 850 hPa on 6th September.

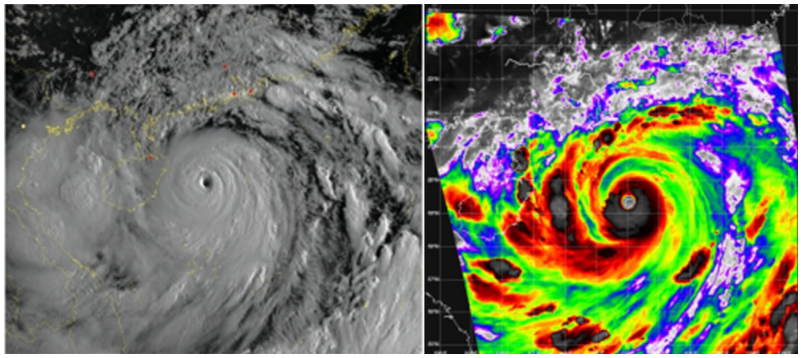

Figure 2. Cloud image of the "Yagi" satellite.

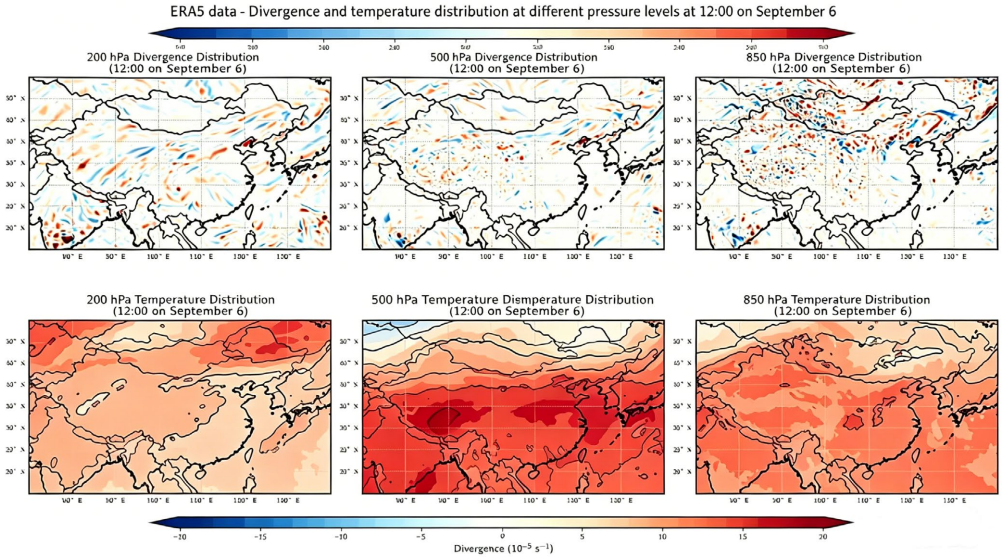

Figure 3. Distribution of divergence and temperature changes in different pressure layers on 6th September, 2024 at 12:0. The geographic base map is derived from the standard map of the Ministry of Natural Resources of the People's Republic of China (Approval No. GS(2025)1685), with no modification to the original map boundaries. Meteorological data are from ECMWF ERA5 reanalysis dataset.

value at 850 hPa reached −6 to $-8 \times 10^{-5} \cdot s^{-1}$, and the divergence center at 200 hPa reached 8 to $10 \times 10^{-5} \cdot s^{-1}$ in **Figure 1**. Moreover, the divergence range in the upper levels was larger than the convergence area in the lower levels, significantly enhancing the vertical upward movement. This dynamic configuration was the core driving force for the typhoon to complete the four-level consecutive jumps from "strong tropical storm" to "super typhoon" within 15 hours.

The satellite cloud in **Figure 2** shows that during this stage, the eye area of the typhoon is clear, and the spiral cloud system is compact, which is highly consistent with the symmetrical distribution of the vorticity field.

From 08:00 to 16:00 on September 6th (before landing in Wenchang, Hainan), the value of the low-level convergence center at 850 hPa reached −6 to $-8 \times 10^{-5} \cdot s^{-1}$ (negative divergence). The convergence area almost completely overlapped with the vorticity center. **Figure 3** shows that the rotational airflow and the convergent airflow were highly coupled, and a large amount of warm and humid air was

drawn into the core area of the typhoon.

Meanwhile, at the 200 hPa level, there is a strong divergence center with a rate of 8 - 10 × 10^{-5}·s^{-1}, and the divergence area is slightly larger than the convergence area at the lower level (with a coverage radius of approximately 6 degrees of latitude). This "strong divergence in the upper layer compared to the convergence in the lower layer" configuration further enhances the suction effect of vertical upward movement, causing the vertical velocity in the eye wall area to reach its peak on September 6th. Within the typhoon eye area (with a diameter of 20 - 30 km), there is a weak divergence zone, corresponding to the descending air flow, which is consistent with the observed fact of "brief clear sky in the eye area" when the typhoon made landfall in Wenchang.

4.2. Thermal Field Warm-Hearted Structure and Humidity Spiral Characteristics

The thermal structure is one of the core internal driving factors for the maintenance and intensification of typhoons. Especially during the three rapid intensification processes of "Yagi", the coordinated evolution of the warm core structure and humidity field exhibited significant asymmetry and vertical stratification characteristics. The horizontal distribution of temperature at various pressure levels extracted based on ERA5 reanalysis data (**Figures 4(a)-(g)**) shows that "Yagi" presented a typical thermal configuration of "warm core in the middle and upper levels, weak warmth in the lower levels, and cold cover in the upper levels" during the super typhoon stage (from 06:00 on September 5th to 22:00 on September 6th).

From the distribution of temperature anomalies in each pressure layer (**Figures 4(a)-(g)**), it can be seen that the warm core structure of "Yagi" is most prominent in the 300 - 500 hPa layer, with positive temperature anomalies generally reaching 3 - 6 K. In some areas of **Figure 4(d)**, the temperature even exceeds 6 K at the 500 hPa layer. This layer overlaps with the main height layer of latent heat release, indicating that the latent heat released by water vapor condensation is the main heat source for maintaining the warm core. In contrast, the positive temperature anomalies in the lower layer (850 - 600 hPa) are only 1 - 3 K (**Figures 4(e)-(g)**), and the horizontal gradient is weak, reflecting that the thermal response in the lower layer mainly relies on the turbulent heat flux in the boundary layer and the sea-air exchange process. **Figure 4(a)** shows that the intensity of the warm core at the 200 hPa level significantly weakens but can still be identified, indicating that the vertical development height of the typhoon is relatively high, and the "cold cap" structure at the top of the convection has not been completely destroyed.

It is worth noting that the horizontal distribution of the warm core shows an approximately concentric circular structure. The maximum temperature value of the center is located in the typhoon eye area, and the temperature rapidly decreases with the increase in radius. Especially near the 500 hPa layer, the temperature gradient between the eye area and the eye wall is the steepest, and the

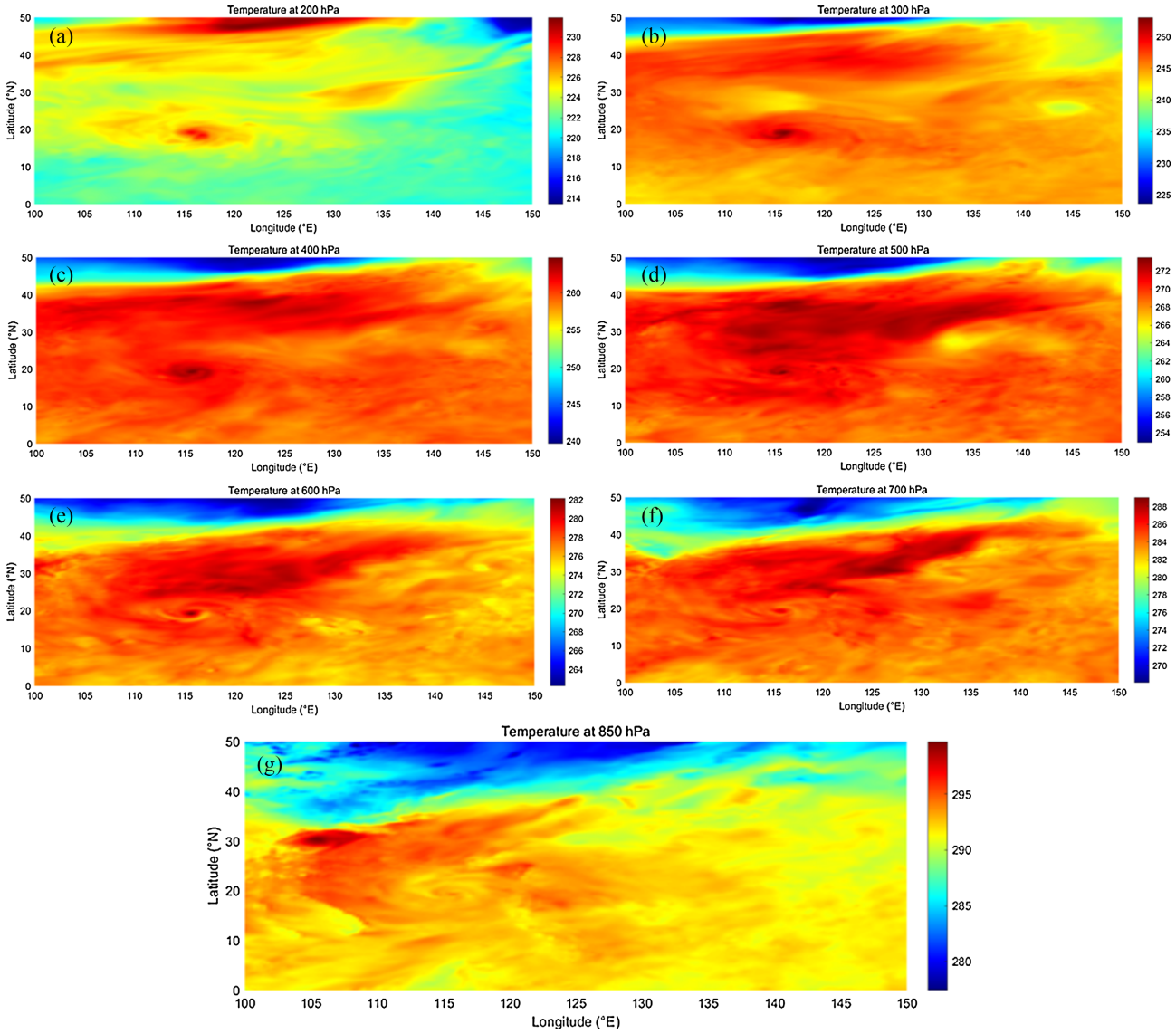

Figure 4. Horizontal distribution of temperature in each pressure layer.

thermal contrast is the most intense. This structure reaches its peak on September 6 at 12:00, corresponding to the peak intensity of the typhoon (68 $m \cdot s^{-1}$). In addition, the center of the warm core has a slight tilt in the vertical direction, which may be related to a slight increase in environmental vertical wind shear around 6 days ago, but the overall tilt amplitude is limited and has not caused a significant separation between the thermal center and the circulation center.

Based on the analysis of the relative humidity fields in each pressure layer (**Figures 5(a)-(g)**), the humidity distribution of "Yagi" presents a typical spiral band structure. The high-humidity areas (RH > 80%) are mainly concentrated in the eye wall and the peripheral spiral rainband region, which is highly consistent with the typhoon circulation pattern. **Figure 5(g)** shows that the relative humidity at the lower level of 850 hPa is relatively low, indicating that dry air is being drawn in from the periphery of the typhoon. This dry-wet alternating spiral band is

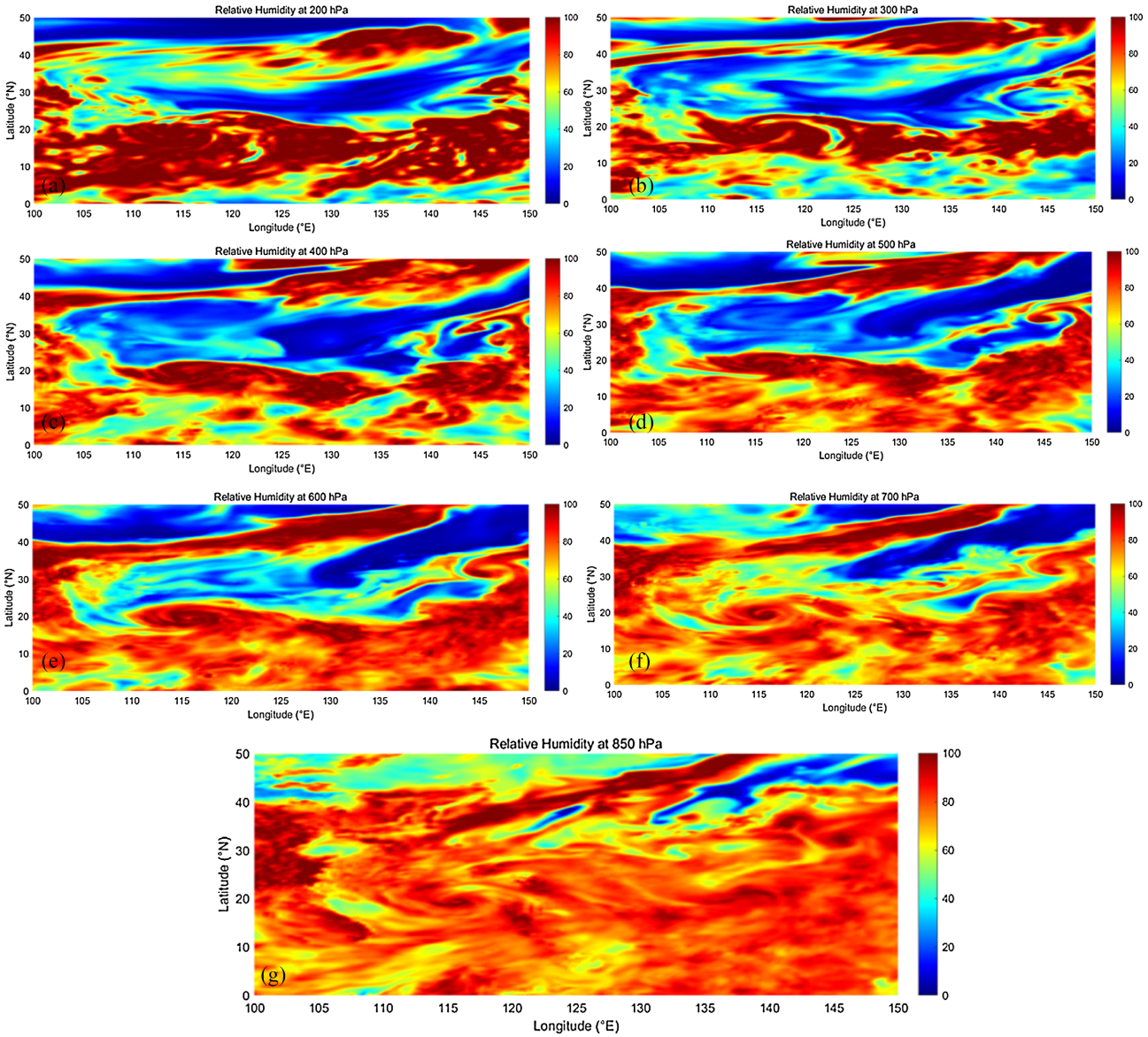

Figure 5. Distribution of relative humidity fields in each pressure layer.

particularly obvious in the 500 - 700 hPa layer (**Figures 5(d)-(f)**), and may have a local inhibitory effect on the convective activity of the eye wall.

At the upper level of 200 hPa, the relative humidity in the eye wall area shown in **Figure 6(a)** is close to saturation (RH > 95%), indicating that the water vapor in the upper outflow layer is abundant, which is conducive to the maintenance of radiative cooling and latent heat release. The relative humidity at the middle layer of 500 hPa remains between 70% and 85% (**Figure 5(d)**), providing good water vapor conditions for the development of deep convection. Overall, the intrusion of dry air mainly occurs in the peripheral area of the lower layer, and has not significantly disrupted the core warm center structure, but its modulation effect on the convective activity of the typhoon periphery is worthy of attention.

By comparing the thermal parameters and intensity changes in the eye wall

area (70 - 100 km from the center), it can be known that the intensity and vertical extension height of the thermal structure of "Yagi" are positively correlated with the maximum wind speed at the center. Starting from 06:00 on September 5th, the intensity of the warm center in the 300 - 500 hPa layer continued to increase, reaching its peak by 12:00 on September 6th, and then the typhoon entered the Beibu Gulf and entered a re-enhancement stage on September 7th. Although Figure (c) shows that the latent heat flux increased again, the intensity of the warm center did not return to the peak level, indicating that the recovery of the thermal structure lagged behind the enhancement of the ocean heat flux.

In addition, the weak inversion zone (maximum temperature layer) in the 300 - 400 hPa layer (temperature maximum layer) indicates the direct manifestation of the concentrated release of latent heat. The existence of this layer significantly reduces the vertical temperature gradient at the center of the typhoon, enhances the overall static stability of the air column, and is conducive to the maintenance and further strengthening of the low-pressure center. This feature is most prominent from 08 to 16:00 on September 6th, which is consistent with the peak intensity height before the typhoon landed in Wenchang, Hainan.

4.3. Quantitative Evolution of Eye Wall Wind Field and Coupling of Intensity

Taking the instantaneous center of the typhoon as the origin, interpolate the Cartesian coordinate grid points to the cylindrical coordinate system (r, θ, p), decompose the tangential wind, radial wind, and extract the vertical velocity. Select the 850 hPa layer in the eye wall area (70 - 100 km from the center), and statistically calculate the key dynamic parameters at 12:00 every day from September 1st to 9th as shown in **Table 1**.

Table 1. Key dynamic parameters of the 850 hPa pressure layer from 1st September to 9th September.

Time (12:00)	Tangential wind speed ($m \cdot s^{-1}$)		
	Maximum	Average	Level
9.1	21.66	13.19	Severe Tropical Storm
9.2	19.83	12.87	Severe Tropical Storm
9.3	24.64	21.42	Severe Typhoon
9.4	33.53	28.92	Severe Typhoon
9.5	41.31	33.37	Severe Typhoon
9.6	43.45	34.52	Severe Typhoon
9.7	36.99	28.06	Severe Typhoon
9.8	11.1	6.43	Tropical Storm or below
9.9	11.74	6.09	Tropical Storm or below

Continued

Typhoon center (latitude and longitude)	Radial wind speed ($m \cdot s^{-1}$)		
	Maximum inflow	Average	Convergence/Divergence
124.50˚E, 13.75˚N	−9.42	0.35	Divergence
122.25˚E, 17.25˚N	−9.20	0.69	Divergence
118.75˚E, 18.75˚N	−5.39	−0.37	Convergence
116.75˚E, 19.25˚N	−9.40	−1.21	Convergence
114.25˚E, 19.25˚N	−6.96	−0.48	Convergence
110.00˚E, 20.00˚N	−13.36	−1.74	Convergence
106.25˚E, 21.25˚N	−11.99	−3.6	Convergence
105.00˚E, 21.75˚N	−6.92	−1.33	Convergence
102.00˚E, 21.50˚N	−12.96	−5.48	Convergence

Select the eye wall area at the 850 hPa level (70 - 100 km from the center), and statistically analyze the key dynamic parameters from September 1st to 9th (negative radial wind indicates inflow, negative vertical velocity indicates upward movement). The results show that the typhoon underwent a complete "development - peak - decay" process. From September 1st to 2nd, it was a strong tropical storm, and on the 3rd, it rapidly intensified to a strong typhoon and maintained this intensity until the 7th. From the 5th to the 6th, it reached its peak intensity, and after landing on the 8th, it rapidly weakened to below the tropical storm level. The tangential wind speed continuously increased from 21.66 $m \cdot s^{-1}$ on September 1st to 43.45 $m \cdot s^{-1}$ on the 6th, and the rotational kinetic energy continuously accumulated; the maximum inflow wind speed reached a peak of −13.36 $m \cdot s^{-1}$ on the 6th, and the intensity of low-level convergence reached its maximum; the negative vertical velocity range was the largest from the 5th to the 6th, and the upward movement was the most intense. During the strong typhoon stage, the environmental wind shear remained at a low value, the typhoon structure was symmetrical, and it was conducive to energy concentration.

Analysis of the three-dimensional structure characteristics of the wind field reveals that the maximum tangential wind speed increased continuously from 21.66 $m \cdot s^{-1}$ on September 1 to 43.45 $m \cdot s^{-1}$ on September 6, and the average tangential wind speed also rose from 13.19 $m \cdot s^{-1}$ to 34.52 $m \cdot s^{-1}$, indicating that the rotational kinetic energy of the typhoon was continuously accumulating. From September 5 to 6, it was the peak intensity period. **Figure 6** shows that the tangential wind speed remained above 40 $m \cdot s^{-1}$.

The radial inflow velocity reached its peak on September 6th at −13.36 $m \cdot s^{-1}$ (negative value indicates inflow), with an average radial wind speed of −1.74 $m \cdot s^{-1}$, indicating that the low-level convergence was the strongest on that day. The intense convergence transported warm and humid air to the eye wall, providing

"fuel" for latent heat release. After September 3rd, the typhoon area changed from divergence to convergence, marking the establishment of the secondary circulation.

The range of vertical velocity (negative value indicates ascent) reached its maximum on September 5 - 6 (−0.0403 to −0.0048 hPa·s^{-1}), with the most intense ascending motion. The eye wall area was dominated by ascent, while the eye area had weak descent (**Figure 7**), forming the typical dynamic structure of a mature typhoon. During the entire strong typhoon stage, the environmental vertical wind shear was very small, which was conducive to the maintenance of the axisymmetric structure.

At 12:00 on September 6th, the center of the typhoon was located at 110.00˚E, 20.00˚N, reaching its peak intensity. The low-level easterly jet stream is obvious, and the radial profile in **Figure 7** shows that the tangential wind, radial wind and

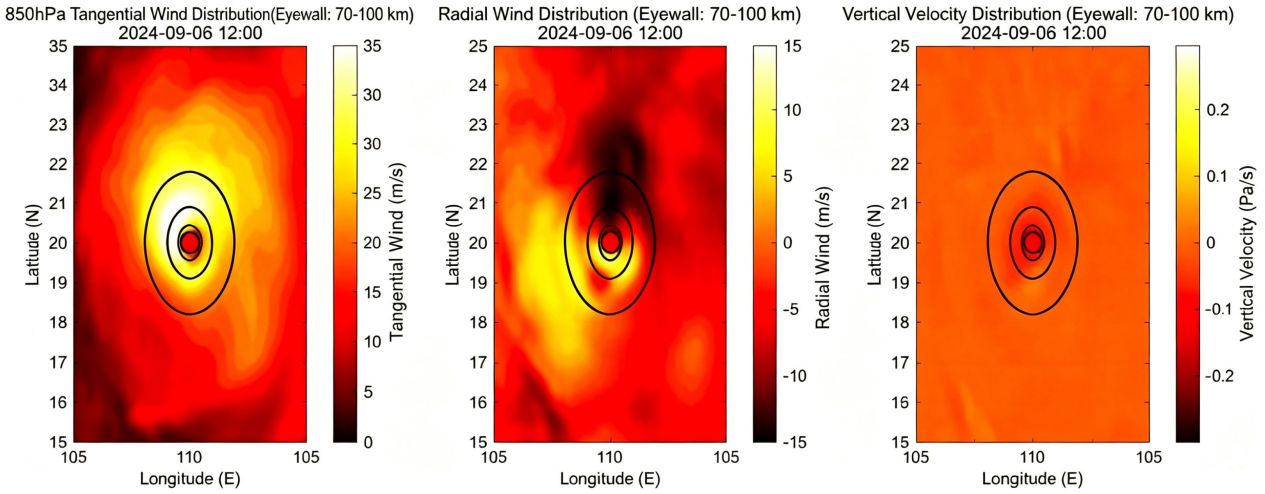

Figure 6. Wind speed distribution map at 850 hPa on 6th September.

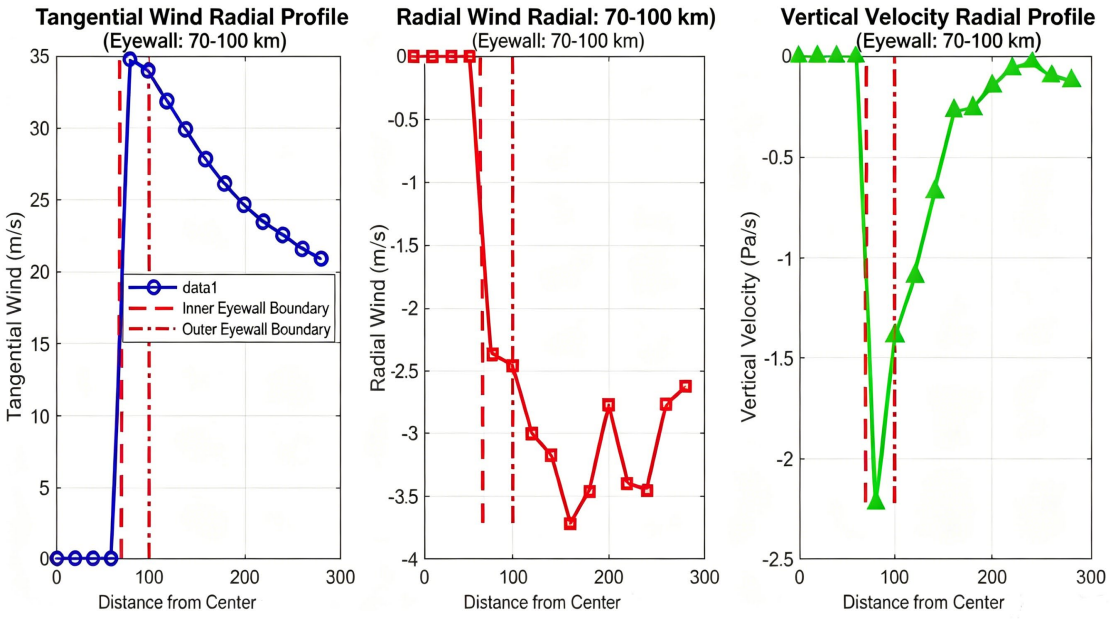

Figure 7. Radial profile structure at 850 hPa on 6th September.

vertical velocity undergo sudden changes at a distance of about 65 km from the center. This precisely locates the eye wall position. At this time, strong convergence at the lower level, intense upward movement of the eye wall, and strong divergence at the upper level form an efficient heat engine cycle. Combined with very small vertical wind shear and warm sea temperature, they jointly support an extreme intensity of 68 $m \cdot s^{-1}$.

4.4. Path Evolution and Mechanism of Guiding Airflow

To quantitatively analyze the dominant role of the environmental airflow on the path of "Yagi", the entire-layer guiding airflow within a 3˚ to 7˚ latitude and longitude range around the typhoon center at 850 to 100 hPa was calculated. The results show that after September 4th, the direction of the typhoon's movement was consistent with the height of the entire-layer guiding airflow, and the vertical weight of the guiding airflow was biased towards the upper levels (500 to 300 hPa), which is related to the strong intensity and high development height of the typhoon.

As can be seen from **Table 2**, throughout the entire lifecycle of the typhoon, the weighted guiding airflow direction at 500 hPa and 850 hPa was consistently east wind, which was in perfect agreement with the actual movement direction of the typhoon (northwest to west-northwest to southwest to west-southwest). The weighted guiding wind speed reached 8.45 $m \cdot s^{-1}$ and 7.47 $m \cdot s^{-1}$ during the peak period from September 5th to 6th, which was the strongest period.

The stability of the guiding airflow, the continuous energy supply from the warm sea temperature, and the weak terrain interference jointly contributed to

Table 2. 500 hPa and 850 hPa pressure layer guiding airflow from 6th September to 9th September.

Time (12:00)	Guide airflow correlation		
	Typhoon center	500 hpa	850 hpa
9.1	124.50˚E, 13.75˚N	7.58	0.28
9.2	122.25˚E, 17.25˚N	3.34	0.83
9.3	118.75˚E, 18.75˚N	4.17	0.18
9.4	116.75˚E, 19.25˚N	4.07	1.29
9.5	114.25˚E, 19.25˚N	3.71	10.48
9.6	110.00˚E, 20.00˚N	6.35	7.94
9.7	106.25˚E, 21.25˚N	2.92	2.53
9.8	105.00˚E, 21.75˚N	0.92	3.43
9.9	102.00˚E, 21.50˚N	0.34	4.29
Time (12:00)	Guide airflow correlation		
	Typhoon center	Weighting ($m \cdot s^{-1}$)	Direction
9.1	124.50˚E, 13.75˚N	2.08	easterly

Continued

9.2	122.25˚E, 17.25˚N	0.42	easterly
9.3	118.75˚E, 18.75˚N	1.38	easterly
9.4	116.75˚E, 19.25˚N	2.12	easterly
9.5	114.25˚E, 19.25˚N	8.45	easterly
9.6	110.00˚E, 20.00˚N	7.47	easterly
9.7	106.25˚E, 21.25˚N	0.89	easterly
9.8	105.00˚E, 21.75˚N	2.67	easterly
9.9	102.00˚E, 21.50˚N	2.90	easterly

the "Yagi" typhoon's unchanging westward path.

Based on the analysis of the experimental results, the core causes of the path stability can be deduced:

- Guiding airflow dominance: The convergence of the easterly airflow on the south side of the subtropical high and the westward airflow on the south side of the continental high locks in the westward path;
- Sea temperature support: The SST in the northern part of the South China Sea exceeds the 26.5˚C threshold (as **Figure 8** shows), and the thickness of the

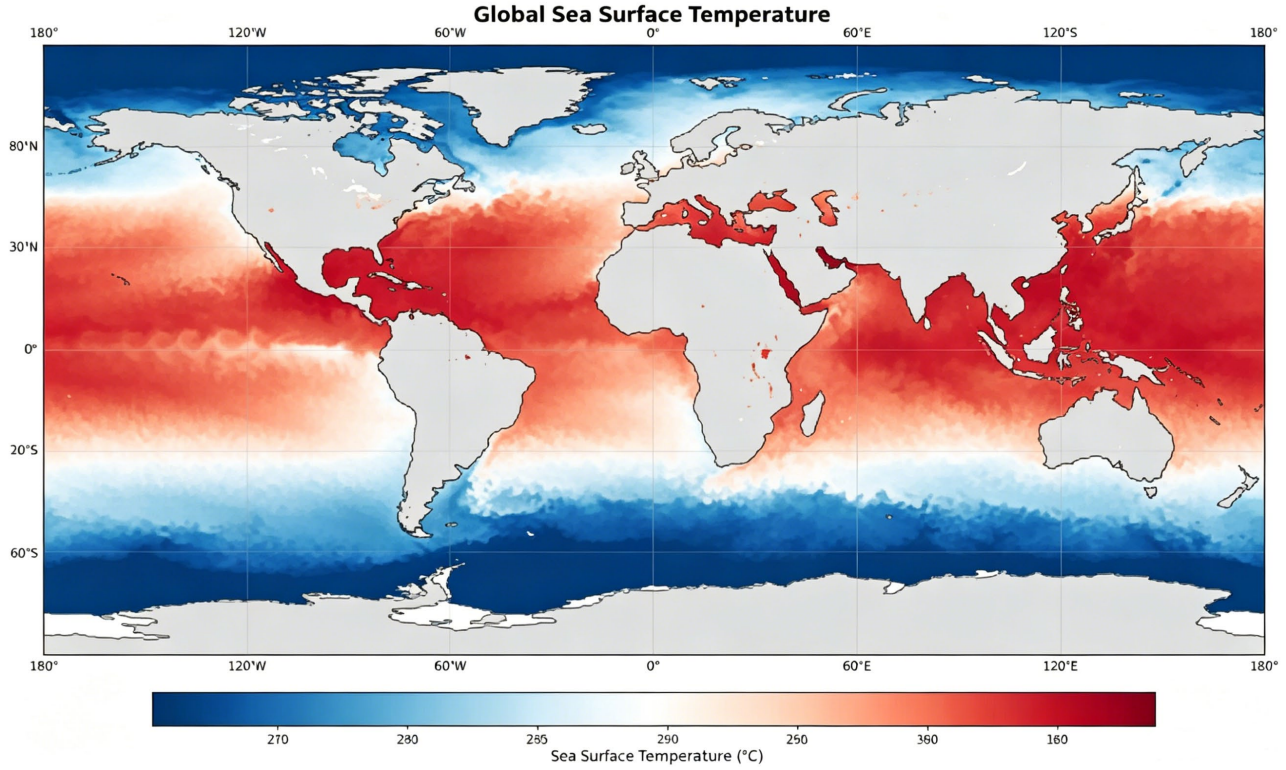

Figure 8. Global sea temperature distribution. The global geographic base map is obtained from the standard world map of the Ministry of Natural Resources of the People's Republic of China (Approval No. GS(2025)1686), with no modification to the original map boundaries. Sea surface temperature data are from ECMWF ERA5 reanalysis dataset.

warm water layer exceeds 50 meters, maintaining the high intensity and structural stability of the typhoon;

- Terrain influence is limited: The terrain of Luzon Island only causes a brief deceleration and a slight northward deviation, and after entering the South China Sea, it quickly resumes the positive westward path;
- Cold air assistance: The strengthening of the weak cold air from the north enhances the low-level convergence, strengthens the typhoon structure, and further stabilizes the path.

5. Conclusion and Discussion

5.1. Core Conclusion

The optimal vertical configuration of thermal-hydraulic coupling is the extreme explosive enhancement mechanism of the "Yagi" core. The synergy of strong positive vorticity in the middle and lower layers and weak negative vorticity in the upper layer, as well as strong convergence in the lower layer and strong divergence in the upper layer, drives the development of efficient secondary circulation and supports the rapid consecutive intensification of the typhoon;

The core area of warming at 300 - 500 hPa and the spiral humidity distribution form a stable thermal support. The intensity of the warm core, the evolution of the eye wall wind field, and the intensity burst of the typhoon show a high positive correlation, and it is a key indicator for the early warning of extremely strong typhoons in the South China Sea in autumn;

The eastward guiding airflow superimposed by the subtropical high and the continental high has absolute control over the path of "Yagi". The abnormal high sea surface temperature in the South China Sea and weak vertical wind shear jointly ensure the stability of the typhoon structure and the long-term maintenance of extremely strong intensity.

5.2. Key Questions Answered

The final answers to the three scientific questions raised in this article are as follows:

- Scientific Question 1: During the rapid intensification of "Yagi", the dynamic field shows a "lower positive and upper negative" vorticity configuration and a "lower convergence and upper dispersion" divergence configuration. The thermal field has a stratified structure of "strong warm center in the middle and upper layers, weak warm in the lower layers", and the vertical coupling driving intensity has erupted;
- Scientific Question 2: In the core area of the eye wall from 70 to 100 km, the tangential wind, radial inflow, and vertical movement reach synchronous peak values, which is highly coupled with the intensity evolution, and is the core feature of the internal core power response of the typhoon;
- Scientific Question 3: The weighted easterly wind from the middle and upper layers dominates absolutely. The subtropical high and the continental high

lock the path together, while the terrain and cold air only play a minor adjusting role.

5.3. Research on Innovation

The core innovation of this paper lies in the construction of a framework integrating dynamics and thermodynamics, three-dimensional wind field decomposition, and integrated analysis of the entire layer of guiding airflow, which enables a systematic analysis of the mechanism of extremely strong typhoons in the South China Sea, quantitatively characterizing the evolution of the wind field in the eye wall core area, and filling the gap in the diagnostic scale of the core of extremely strong typhoons in the South China Sea during autumn.

5.4. Future Outlook

Future research can be conducted along the following directions: 1) Conduct a comparative energy budget analysis of "Yagi" and similar historical typhoons (such as "Wesmas" and "Squirrel"); 2) Utilize high-resolution large-eddy simulation (LES) to reveal the mesoscale processes between the eye wall convective burst and the kinetic energy generation term; 3) Develop an objective forecast model for typhoon intensity based on the combination of fractal dimension and deep learning. These efforts will help further enhance the forecasting capabilities of typhoons in the South China Sea, especially those that rapidly intensify, and provide more solid scientific support for disaster prevention and mitigation.

Acknowledgements

We thank the data support from ECMWF and the National Meteorological Information Center of China. We also thank the College of Meteorology and Oceanography, National University of Defense Technology, for the research conditions.

Conflicts of Interest

The authors declare no conflicts of interest regarding the publication of this paper.

References

Chen, H. Y., Yu, X. F., Zhang, Y. L. et al. (2026). Evolution of Fractal Characteristics of Typhoon Yagi and Its Relationship with Wind Speed. *Journal of Applied Oceanography*, *45*, 227-235. (In Chinese) https://www.xueshuwenhai.com/yyhyxxb

Chen, L. S., & Ding, Y. H. (1979). *Introduction to Typhoons in the Western Pacific.* Science Press.

Ford, M. R., & Kench, P. S. (2014). Formation and Adjustment of Typhoon-Impacted Reef Islands Interpreted from Remote Imagery: Nadikdik Atoll, Marshall Islands. *Geomorphology*, *214*, 216-222. https://doi.org/10.1016/j.geomorph.2014.02.006

Ford, M. R., & Kench, P. S. (2016). Spatiotemporal Variability of Typhoon Impacts and Relaxation Intervals on Jaluit Atoll, Marshall Islands. *Geology*, *44*, 159-162. https://doi.org/10.1130/G37402.1

Liang, H. L., & Cheng, Z. Q. (2017). Analysis of Causes for Differences in Precipitation of

Two Typhoons Affecting Yunnan with Similar Tracks in 2014. *Meteorological Monthly*, *43*, 1339-1353. (In Chinese)

Liang, L., & Wu, Z. W. (1986). Kinetic Energy Budget of the Development of Offshore Typhoons in the East China Sea. *Journal of Tropical Meteorology*, *No. 2*, 125-134. (In Chinese)

Oh, Y., Moon, I. J., & Lee, W. J. (2015). Typhoon Intensity Consensus Predictions Based on Various Performance Evaluations for Guidance Models. In *Proceedings of the Korean Meteorological Society Conference* (pp. 696-697). Korean Meteorological Society.

Toyoda, M., Mori, N., Kim, S. et al. (2025). Assessment of Climate Change Impact on Compound Flooding Considering Typhoon Intensification and Astronomical Tide in Ise Bay, Japan: A Typhoon Track Ensemble Approach. *Coastal Engineering Journal*, *67*, 379-393. https://doi.org/10.1080/21664250.2025.2500122

Velden, C. S., & Leslie, L. M. (1991). The Basic Relationship between Tropical Cyclone Intensity and the Depth of the Environmental Steering Layer in the Australian Region. *Weather and Forecasting*, 6, 244-253. https://doi.org/10.1175/1520-0434(1991)006<0244:TBRBTC>2.0.CO;2

Wu, M., Wu, Y., Liu, B. J. et al. (2026). Analysis on Early Track Forecast Bias of CMA Numerical Model for Super Typhoon Yagi (2411). *Marine Forecasts*, *43*, 79-88. http://www.hyyb.org.cn/Magazine/Show.aspx?ID=3707

Yan, J. Y., Zhang, X. Z., Chen, Q. J. et al. (1995). The Standard of Rapidly Intensified Tropical Cyclones. *Meteorological Monthly*, *21*, 9-13. http://qxqk.nmc.cn/qx/ch/reader/view_abstract.aspx?file_no=19950502&flag=1

Yang, G. J., Han, P. C., Cheng, Z. Q. et al. (2026). Characteristics and Causes of Abnormal Intensity Changes of Super Typhoon Yagi. *Meteorological Monthly*, *52*, 16-28. (In Chinese)

Yu, Y. B., Yang, C. X., & Yao, X. P. (2007). Analysis on Vertical Structure Characteristics of Intensity Abrupt Change of Offshore Tropical Cyclones. *Chinese Journal of Atmospheric Sciences*, *31*, 876-886. (In Chinese)